RESEARCH PAPER

PCCP
www.rsc.org/pccp

Layered structures of shear-oriented and multilayered PEO/silicate nanocomposite films

Matthew M. Malwitz,[a] Avinash Dundigalla,[a] Vincent Ferreiro,[b] Paul D. Butler,[c] Margaret C. Henk[a] and Gudrun Schmidt*[a]

[a] *Department of Chemistry, Louisiana State University, Baton Rouge, LA 70803, USA. E-mail: gudrun@LSU.edu; Fax: 225 578 3458; Tel: 225 578 7375*
[b] *Laboratoire de Structure et Propriétés de l'Etat Solide, UMR CNRS 8008, Université des Science et Technologie de Lille, Villeneuve d'Ascq, France*
[c] *Oak Ridge National Laboratory, Oak Ridge TN 37831, USA*

Received 9th February 2004, Accepted 8th April 2004
First published as an Advance Article on the web 16th April 2004

The structure and orientation of polymer and clay platelets in multilayered, micrometer-thick nanocomposite films was investigated by means of scanning electron microscopy (SEM), atomic force microscopy (AFM), optical microscopy and small-angle neutron scattering (SANS). Microscopic and scattering methods complementarily measured the morphology and shear-induced orientation of polymer and platelets in films when spread layer by layer from a network-like polymer clay solution. During the drying process, the polymer clay network collapsed and clay platelets oriented inside the network with the clay surface normal perpendicular to the spread direction (x–z plane). On nanometer length scales, SANS and AFM yielded structure and orientation of platelets and polymer in and perpendicular to the spread direction of the film. SEM investigations led to the observation of unexpected morphology on the micron length scale. SEM did not detect boundaries between single spread, micron-thick film layers but, surprisingly, showed a highly ordered and layered structure of the film. Polarized light microscopy showed differences in birefringence in each plane.

Introduction

Polymer clay nanocomposites are hybrid materials that exhibit a change in composition, structure and properties over the scale of nanometers.[1] Ordering layered silicates with high aspect ratio at the nanometer length scale is a challenging and active research area in materials science and engineering.[2–8] Approaches developed so far range from manipulation of individual particles to exploitation of self assembly in colloids.[9,10] The large aspect ratio of platelets promotes a supramolecular organization similar to other mesoscopic systems such as liquid crystalline polymers,[11–14] surfactants[15] or block copolymers.[16,17]

The effect of shear on the orientation of polymer nanocomposites has been examined by a number of groups[18–22] and in some cases the three-dimensional orientation of the polymer and clay has been determined.[23] Small and wide angle scattering and microscopy are powerful techniques used to characterize structure and orientation. For example, poly(ethylene oxides) PEO-clay blends have been investigated and accelerated crystallization and clay induced orientation of PEO crystallites has been observed.[24,25] Earlier work has found that intercalation of PEO within galleries of clay resulted in hybrid structures that can accommodate a maximum ratio of polymer to clay and any excess polymer leads to the formation of two phases: either polymer-clay intercalates or pure polymer phases.[26,27] More recent transmission electron microscopy (TEM)[28] has revealed a house of cards structure in nanocomposite melts under elongational flow. Strong strain induced hardening and rheopexy features at higher deformation originate from the perpendicular alignment of the clay to the stretching direction. TEM can reveal the difference in the shear flow induced *versus* elongational internal structures of the nanocomposite which is important in making films.

There are several different nanocomposite fabrication techniques that vary from intercalation to exfoliation in solution as well as the polymer melt. The structure and mechanical properties of PEO in aqueous solutions have been found to penetrate into montmorillonites and strongly promote the exfoliation process. In a few cases an interlayer helical conformation was reported for polymer molecules such as PEO.[1,29] When polymer solutions are added to exfoliated clay dispersions the strong interactions between the two components often leads to re-aggregation which is difficult to overcome.[30] In the "wet state" of an exfoliated polymer clay gel or after air drying, the silicate layers remain trapped in the gel-like polymer film.[1] The film quality can be improved by slow evaporation of the solvent where the clay platelets have time to assemble under gravitational and osmotic forces before the viscosity of the system impedes particle realignment.[25,31] An industrial more promising way is the melt intercalation of PEO into montmorillonites where polymer chains were found to be more effectively intercalated than *via* solution.[26,32,33] The reason was that water is a good solvent for PEO and the polymer water interactions impede complete intercalation.[26,32,33]

There has been new technology of adsorption from solution[34] for the fabrication of molecularly ordered multicomposite films in order to expand and replace the well known Langmuir–Blodgett techniques and to open the field of molecular self assembly to materials science.[35,36] For example, atomic force microscopy[34] on multilayered clay films revealed that polymer Laponite films are characterized by significantly higher surface coverage than natural clays such as Montmorillonite. These films as well as those studied by Kleinfeld *et al.*[37] were prepared by sequential adsorption of polymer and clay.

Previous work relevant to this paper described a rheological and small angle neutron scattering study (SANS) on network like solutions of clay and poly (ethylene oxide).[38–41] The

DOI: 10.1039/b401892c

polymer and the clay interact in a dynamic adsorption/desorption equilibrium to form a 3D network.[41] The mesh size of this 3D network and the orientation in solution is important to the structure of dried films. Our work also focused on the orientation of platelets in multilayered polymer–Laponite films, as studied by small and wide angle scattering.[42]

The objective of the present contribution is to use network-like polymer–montmorillonite solutions[38] to prepare nanocomposite films with a defined orientation of the clay platelets and determine how the shear-orientation in the solution influences the film structure after the solvent is evaporated. Only completely dry films will be investigated. Efficient nanoparticle dispersion in solution combined with good polymer/particle interfacial adhesion allows the exciting possibility of developing network-like films, tissues or very porous membranes. Porosity strongly depends on the sample preparation conditions. On a nanometer length scale, SANS and AFM are complementarily used to study the structure and shear-induced orientation of polymer and platelets after a film is spread and dried from a network-like polymer clay solution. SEM and microscopy investigate the morphology and porosity of the films on a micron length scale. Hybrid films, such as the ones described in this paper, offer a range of challenges and opportunities.

Experimental

Natural clay montmorillonite (Cloisite NA+, CNA) (Southern Clay Products) was used in this study. The clay consists of platelets that range in size from 700 to 1500 Å across and *ca.* 10 Å in thickness and a clay polydispersity of *ca.* 30 % according to the supplier. Poly(ethylene oxide) ($M_w = 10^6$ g mol^{-1}, molecular weight distribution *ca.* 1.5) was purchased from Polysciences, Inc. Films were prepared *via* solution exfoliation. Optimal solutions are obtained for a particular polymer clay ratio, the pH and ionic strength as described by Malwitz *et al.*[38] All the results reported here are from multilayered films that have been made from a solution containing mass fractions of 3% CNA clay and 5% PEO at ambient temperature. The CNA clay produces an opaque suspension of predominantly "exfoliated" platelets (no peaks at high q in SANS). The quiescent or equilibrium structure is that of a homogeneous solution with near ideal polymer and clay solution and good adhesion between the polymer and the clay. Due to the relatively high polymer and clay concentrations, we expect that randomly oriented domains of oriented polymer covered clay particles are present. Both the pH and the ionic strength of the solution were controlled by the addition of NaOH (pH = 10) and NaCl (3 mM), respectively. Under these conditions, flocculation and degradation of the clay particles are avoided. Sample preparation can be reduced to 3 weeks when samples are mixed/sheared and centrifuged daily. Simply dissolving the polymer and the clay in water is not sufficient to completely exfoliate the samples. Instead, extensive mixing and shearing are necessary to assure sample reproducibility. All solutions used for making films were confirmed to be exfoliated, homogeneous and stable.

Solutions were spread on glass slides, layer by layer and dried at 25 °C in desiccators and under vacuum. Multilayered films containing *ca.* 33% of clay and 67% of PEO polymer were obtained. Preliminary annealing studies and thermogravimetric analysis indicate that water is dried out of the films ($\ll$0.5%). More detailed film preparation is described under references[42] and notes.[43] Multilayered films with an average layer thickness of *ca.* 5–7 μm were obtained by manually spreading the filled polymer gel on a glass substrate with a blade. Films with the same spread direction were dried layer by layer onto each other until a total multilayer film of *ca.* 1–2 mm was obtained. The simple preparative method used by us offers a powerful strategy to building ordered films by shear orientation from solution. One reason why we chose the spreading and drying procedure is the high modulus of the 33% clay polymer nanocomposites, which made shear orientation in the bulk with conventional rheological instrumentation difficult. Spin-casting or dipping of the gum-like hydrogel was problematic due to high viscosity and elasticity, as well as impurities, which were hard to remove.

SANS experiments utilized the 30 m SANS instrument, NG7 at the Center for Neutron Research at the National Institute of Standards and Technology.[44] In a standard configuration, referred to as the y-beam configuration, the incident beam is perpendicular to the spread direction of the film and we obtain SANS intensity in the x–z plane. In a second configuration, referred to as the z-beam configuration, the incident beam is parallel to the spread direction of many stacked films. The neutron beam in z-beam configuration gives SANS intensities in the x–y plane (Fig. 1). ($q = 4\pi/\lambda \sin(\theta)/2$) for 0.0008221 Å^{-1} $< q <$ 0.08621 Å^{-1}. The primary contrast in the SANS experiment is between the silicate and PEO. This allows SANS experiments to detect the overall orientation of the clay platelets in the polymer matrix. Voids and porosity of the network like film structure may influence total scattering intensity.

Optical microscopy was performed with an Olympus BX51TF microscope under crossed polarizers. A small section of a one layer film was removed (by scratching) to expose both the x–z and the x–y plane and to compare results with those obtained from the complementary techniques.

SEM experiments were performed with a Cambridge 260 Stereoscan Electron Microscope. Several bulk film samples were first frozen in liquid nitrogen, then fractured, attached to an SEM stub and coated with gold/palladium in an Edwards S-150 sputter coater. Fractures in all 3D planes have been investigated and only representative images are presented.

Sample preparation for AFM included cryo-fracture and cryo-ultramicrotom slicing. Samples from both methods showed same morphology and structure when investigated. Here, representative AFM results from the dried and cryo-fractured samples are presented. All AFM experiments have been carried out in air at room temperature using a Nanoscope III Multimode Microscope from Digital Instruments operating in the tapping mode to minimize the sample distortion due to mechanical interactions between the AFM tip and the surface.[45] Integrated silicon tips with a radius of curvature of about 10 nm and cantilevers with a nominal spring constant of 30 N m^{-1} have been used.[46] In the tapping mode, the cantilever oscillates vertically at a drive frequency close to its resonance frequency and contacts the sample surface briefly in each cycle of oscillation. As the tip approaches the surface, the vibrational

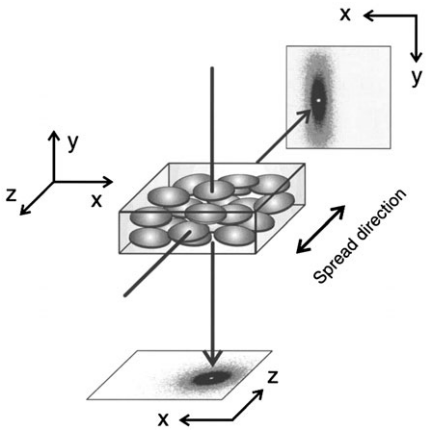

Fig. 1 With the clay platelets aligned in the spread direction of the film (x–z plane) we observe an anisotropic SANS pattern with the neutron beam in z-configuration and an isotropic SANS pattern with the beam oriented in y-configuration.

characteristics of the cantilever oscillation (*e.g.*, amplitude, resonance frequency and phase angle) change due to tip–sample interactions. The surface can be imaged in different ways. "Height" images are obtained by using the feedback loop which keeps the amplitude at a constant value A_{sp} by translating vertically the sample with the piezoelectric scanner. The feedback loop is controlled by the set-point amplitude ratio $r_{sp} = A_{sp}/A_0$ where A_0 is the amplitude of free oscillation.[25–27] The recorded "height" images are the vertical displacements of the piezoelectric scanner. AFM images were recorded with the highest sampling resolution, that is, 512 × 512 data points.[47] Duplicate measurements on all instruments show excellent reproducibility.

Results and discussion

The overall properties of the dried polymer clay nanocomposite films depend on structural features such as morphology, polymer–clay interaction and orientation on a nanometer length scale. In a previous work on solutions we found the polymer chains to be entangled with the clay particles to form a network. Individual long polymer chains can physically absorb to several particles in solution resulting in strong bridging effects and thus enhanced properties in the dried film. When clay particles strongly absorb to the surrounding polymer chains in solution, the polymer does not provide a continuum medium for particle support any more. The network character of the solution can be described as water-rich and nanocomposite rich regions which can be visualized by freeze fracture SEM. Preliminary SANS data over a large q range confirm that polymer–clay solutions have large scale structures that could be described as interconnected networks on several length scales. The structure in solution strongly influences the morphology of the dried film when the water is evaporated and these networks collapse. The complexity of these nanocomposites makes them extremely tunable through small changes in the chemistry and structure of the polymers.[38] The polymer molecular weight strongly influences the density and strength of the polymer clay bridges and makes shear orientation during the spreading process easy. The orientational alignment of clay platelets is a competition between flow alignment and configurational relaxation during shear. At a given shear rate the relaxation process is hindered by a coupling between the polymer and the clay. Rheological experiments on PEO–CNA solutions (those used for making the films) have shown that the CNA clay platelets already align at shear rates below 5 s^{-1} and after cessation of shear relax from that alignment very slow (within many hours).[48] Evaporation of the solvent at ambient temperature combined with shear orientation strongly improved the film quality and increased the orientation of clay platelets that are layered between polymer.

SANS and AFM

The orientation of the clay platelets in the dried film can be deduced from SANS results and a simple physical picture is illustrated in Fig. 1. The isotropic pattern in the x–z plane and the relatively large anisotropy observed in the x–y plane suggest that the predominant orientation of platelets is with the surface normal perpendicular to the film plane (x–z plane) (Figs. 1 and 2). The SANS intensity is averaged from 10° sectors in the horizontal (x) and vertical direction (y or z) of the 2D SANS pattern with the intensity averaged in horizontal x-directions overlapping (Figs. 1 and 2). This procedure allows the SANS intensities in all three directions to be compared. A shoulder at $q_{max} \approx 0.01$ Å^{-1} corresponds to a d-spacing, $d_{SANS} = 2\pi/q_{max}$, on the order of *ca.* 63 nm and is related to a distance between clay rich areas and polymer rich areas (SANS contrast between polymer and clay). The collapsed network structure from solution must lead to highly oriented layers in the dried film. The d spacing obtained from SANS ($d_{SANS} \approx 63$ nm) is more or less consistent with the spacing of the striped texture measured from AFM $d_{AFM} \approx 56$ nm (average over many measured spacings from several AFM images, see Fig. 3). It is very important that the films are completely dry. The clay, as well as the polymer component are hygroscopic and the reversible absorption/desorption of water leads to swelling/shrinking of the polymer, and thus to increasing/decreasing of layer spacing. This is a property that makes the material applicable as potential humidity sensor.[49]

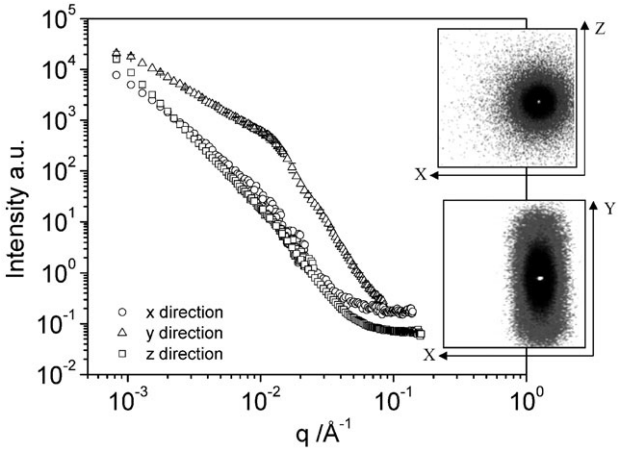

Fig. 2 SANS intensity as averaged in 10-degree sectors for all three directions in space. Isotropic SANS data are circularly averaged. In this case, intensities in z and x directions are the same. Intensities in x direction or circularly averaged data cover a larger q range than intensities in y or z direction. This is due to an off-centered beamstop. Data were placed on the same arbitrary scale.

The anisotropic SANS pattern (Fig. 2) can be well correlated with the Fast Fourier transform AFM data (Fig, 3a, b and c) showing that a broad anisotropic streak in diagonal (Fig. 3, right) is perpendicular to the striped texture (Fig. 3, left). On similar length scales, both methods complement each other. While SANS yields reciprocal space information and an average degree of orientation, AFM visualizes real space structures within discrete sections of the sample. Therefore, slight differences in d_{AFM} and d_{SANS} spacing are to be expected. The existence of the high ordered and layered structure observed with AFM is unusual and unexpected. The orientation and size of the clay platelets which are *ca.* 100 nm in diameter and 1 nm thick, does not explain the highly ordered layers and their thickness of *ca.* 56 nm (Fig. 3). We note, however, that the clay can adsorb only a maximum amount of polymer till all the clay surfaces are covered. Any excess polymer in solution, as well as in the bulk leads to formation of two nanocomposite phases: network like polymer–clay intercalates and pure polymer phases.[26,27] We assume that during the drying process, these two phases lead to the layered structure observed with AFM and SANS. Also of note is that this interpretation is consistent with similar behavior reported by Vaia *et al.*,[26,27] Wu *et al.*[26,27] and Schmidt *et al.*[39]

The anisotropic SANS scattering pattern can be characterized in terms of peak heights and widths of azimuthal intensity profiles in which the peak height is used to assess the changes in molecular orientation or using Herman's function[50–52] to calculate f, the degree of orientation. A system is completely aligned when $f = 1$ and random when $f = 0$. For multilayered films studied in this paper a value of $f = 0.49$ was obtained. As for now SANS contrast of our samples is between the polymer and the clay and cannot distinguish between the orientation of each component, thus limiting the usefulness of shear simplified analysis of form factors. Planned contrast matching studies with deuterated polymer will help interpret these differences and separate scattering contributions from clay and polymer.

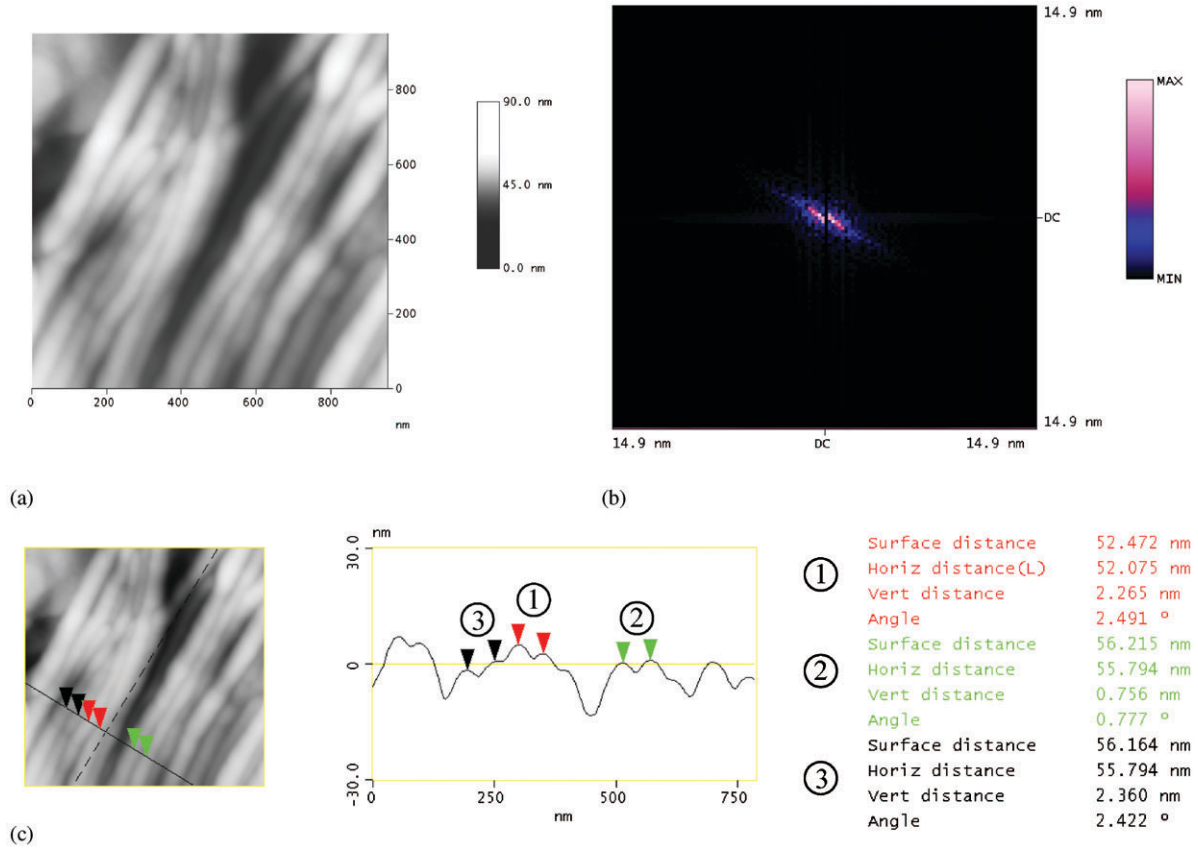

Fig. 3 Representative AFM data from the x–z plane sections of multilayered films. (a) (952 × 952 nm) AFM "height" image of the x–z plane sections of multilayered films. The AFM experimental conditions were: $A_0 = 54$ nm; $f_0 = 179\,788$ Hz; $A_{sp} = 52$ nm with $f_{sp} = 179\,572$ Hz; z-range = 90 nm; (b) FFT spectrum of Fig. 3a; (c) cross section of Fig. 3a.

Scanning electron microscopy. (SEM) determined morphology on a micron length scale. A nanometer scale resolution as obtained with AFM is not achievable with the SEM instrument. As mentioned before, the polymer clay solutions have fractal structures that can be described as interconnected networks on several length scales. When the solvent is evaporated the network collapses (like a squeezed sponge) and we obtain layered structures that can be observed on several length scales (nm resolution given by AFM and micron size observed by SEM). In the y–z plane (Fig. 4a) SEM was used to examine whether an interface exists between each layer. No boundaries between spreading layers could be detected by SEM, indicating substantial intermixing of spread layers while preserving the platelet orientation. Surprisingly, a highly ordered and layered structure of the films has been observed in the x–y plane and porous structures in the x–z plane. The porous structure in the x–z plane (Fig. 4b) appears to consist of interconnecting areas of film and fibers that form a porous mesh or network. From the x–z image we observe polymer fibers that, on average, are about 2050 ± 280 nm in length and approximately 170 ± 10 nm in width with random orientation. These fibers contain both polymer and nanoclay and no such fibers could be obtained with either pure PEO or clay. The clay particles serve as cross linking points within the polymer nanocomposite and lead to improved properties. The layered texture of the x–y SEM image was calculated to have an average dimension of

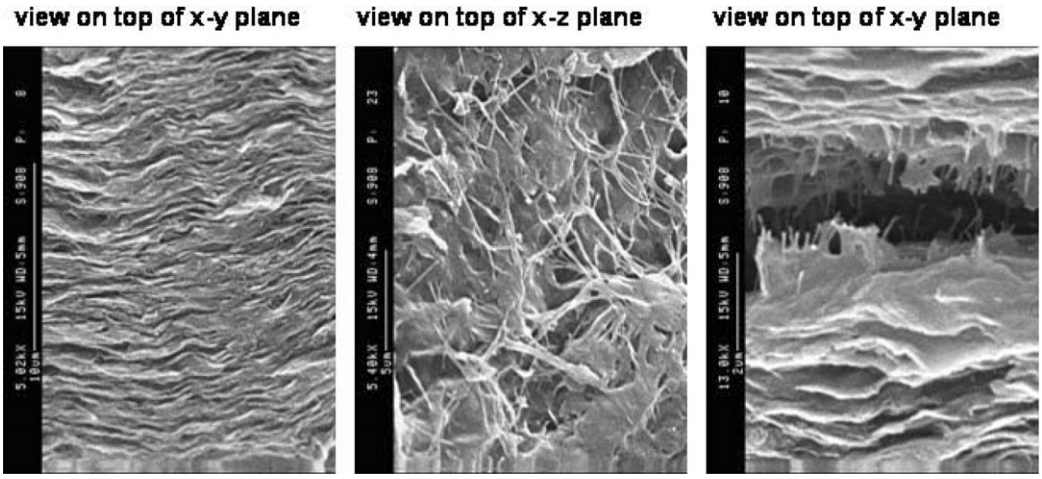

Fig. 4 SEM images of freeze fracture surfaces: (a) view on top of the x–y plane; (b) view on top of x–z plane; (c) view on top of x–y plane and fracture. Planes are described in Fig. 1. Fracture of the film shows part of the network like structure which holds layers together suggesting strong interconnectivity between layers and between the polymer and the nanoclay.

$d_{SEM} = 394 \pm 42$ nm per layer or roughly two times the width of a fiber observed in the x–z plane. According to AFM and SANS measurements, each of the 390 nm thick layers (measured by SEM) must consist of a bundle of smaller layers which are, on average, 55 nm thick. One has to investigate several AFM images in horizontal and vertical distances to observe these bundles. The layers observed by SEM are considerably smaller than the calculated width of a single layer spread to form the nanocomposite film. Further SEM studies suggest that the exact thickness of one dried layer is not as important to the overall orientation of polymer and platelets as, *e.g.*, the "shear rate" during the spreading process and the drying procedure. Fracture of the film (Fig. 4c) shows part of the network like structure which holds layers together suggesting strong interconnectivity between layers and between the polymer and the nanoclay. During the drying and spreading process the polymer clay network collapses and clay platelets are shear-oriented preferentially in the spread direction. We conclude that the strength of the polymer clay network in solution strongly influences the alignment of polymer and clay during the spreading process. In solution, a high degree of porosity is available between the polymer-clay matrix and water filled channels.[38] The collapse of the network during the spreading and drying process of films reduces the pore sizes and the shear leads to orientation and anisotropy. The spreading and drying procedure influences both the micro- and macrostructure.

Optical microscopy. Polarizing microscopy showed differences in birefringence in each plane, x–z and x–y (Fig. 5). A small section of a one layer film was removed (by scratching) to expose the x–y plane. Observation of the x–z plane shows a lightly speckled pattern. This speckling is primarily due to the birefringence observed from PEO crystallites present in the sample. With increasing temperatures in a range from 25 to 200 °C the birefringence gradually disappears due to melting of the polymer crystallites. Observation of the exposed edge of the film, the x–y plane, shows a highly birefringent pattern even after annealing an hour at 200 °C. The total birefringence of the film is dominated by the orientation of the clay platelets and the polymer within the sample. At high temperatures we believe that birefringence comes from the clay alone while at low temperatures both polymer and clay contribute to total birefringence. Previous work on PEO nanocomposites have shown that it is difficult to significantly increase the intergallery distances by adding more polymer to the system and that excess polymer will phase separate upon removal of water.[25] With our polymer nanocomposites, both the pH and the ionic strength of the solutions were controlled by the addition of NaOH and NaCl, respectively. As the water evaporates during the film preparation, the electrolyte concentration increases, causing phase separation of PEO at higher concentrations. The presence of salt may be in part responsible for the development of the layered structure. Optical microscopy data suggest that our nanocomposites do contain some PEO crystals that may have phase separated during the drying and spreading process. Neither high molecular weight polymer nor shear was sufficient to completely overcome phase separation and crystallization of PEO. We also note that there is time required for crystallinity to be observed (*ca.* 3 weeks), however after some time (0.5 years) crystallinity of 55% does not change any more. The crystallinity of PEO various nanocomposites has been studied in the past.[24,25,53] The confinement induced crystallinity is very important in controlling the structure in our multilayered films, an aspect that will be investigated in more detail elsewhere.

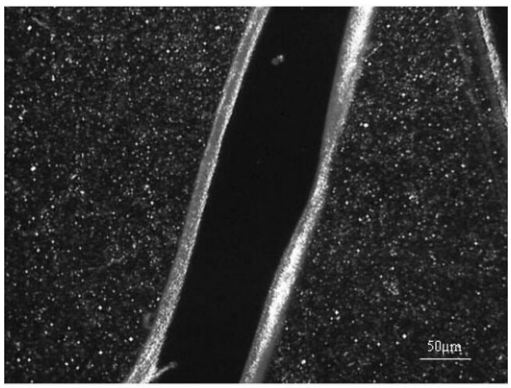

Fig. 5 Optical micrograph of a spread nanocomposite film with scratched surface. A small section of a one layer film was removed (by scratching) to expose the x–y plane. Crossed polarizers and a magnification: 20× were used.

Conclusions

Nanocomposite multilayered films were studied with a combination of scattering and microscopy. The length scales covered by these techniques provide information about short range packing as well as long range correlations. The multilayered films were formed by a layer by layer spreading method from a network like solution. No boundaries between spreading layers could be detected by SEM, indicating substantial intermixing of spread layers while preserving the platelet orientation. During the drying process, the polymer clay network collapsed and clay platelets oriented inside the network with the clay surface normal perpendicular to the spread direction. On a nanometer scale the clay can adsorb only a maximum amount of polymer till all the clay surfaces are covered. Any excess polymer in solution as well as in the bulk leads to formation of two phases: network like polymer–clay intercalates and pure polymer phases. We assume that these two phases lead to the unusual and unexpected layered structure observed with AFM and SANS. We also note that this interpretation is consistent with similar behavior reported in literature.

Our unexpected results pose many open questions and more experiments are necessary for better understanding the origin and nature of the layered structures for a more quantitative evaluation. Planned SANS measurements may help determining the thickness and density of the polymer–clay interfacial regions, the average number of contacts per chain and per particle. Once we have obtained this information, we can determine how the polymer–clay interactions influence the macroscopic behavior and quantify the origin of observed layers. Future X-ray, AFM and SEM investigations in the wet state will help to determine how the layered structure developed when solvent is evaporated slowly. Planned dynamic testing will lead to further elucidation of the rheological behavior in order to better understand viscoelasticity, relaxation and interaction based phenomena.

Acknowledgements

We acknowledge financial support from an NSF-CAREER award, DMR 0348884, from a Louisiana Board of Regents grant, LEQSF (2002-05)-RD-A-09 and from our NSF-IGERT program at LSU. We also acknowledge the support of NIST and the NSF, through agreement no. DMR 9986442 in providing the neutron research facilities used in this work. Oak Ridge National Laboratory is managed for the US Department of Energy by UT-Batelle LLC under contract No. DE-AC0500OR22725. Finally we thank the reviewers for their helpful comments.

References

1 G. Lagaly, *Appl. Clay Sci.*, 1999, **15**, 1–9.
2 R. Krishnamoorti and R. A. Vaia, *Polymer Nanocomposites*, ACS, Washington DC, 2002, vol. 804.

3 J. C. P. Gabriel and P. Davidson, *Adv. Mater*., 2000, **12**, 9.
4 G. Schmidt and M. M. Malwitz, *Curr. Opin. Colloid Interface Sci*., 2003, **8**, 103–108.
5 R. Krishnamoorti and K. Yurekli, *Curr. Opin. Colloid Interface Sci*., 2001, **6**, 464–470.
6 P. Aranda, Y. Mosqueda, E. Perez-Cappe and E. Ruiz-Hitzky, *J. Polym. Sci., Part B: Polym. Phys*., 2003, **41**, 3249–3263.
7 J. W. Gilman, *Appl. Clay Sci*., 1999, **15**, 31–49.
8 P. Reichert, B. Hoffmann, T. Bock, R. Thomann, R. Mulhaupt and C. Friedrich, *Macromol. Rapid Commun*., 2001, **22**, 519–523.
9 J. C. P. Gabriel, F. Camerel, B. J. Lemaire, H. Desvaux, P. Davidson and P. Batail, *Nature (London)*, 2001, **413**, 504–508.
10 G. Lagaly and S. Ziesmer, *Adv. Colloid Interface Sci*., 2003, **100**, 105–128.
11 K. Hongladarom, V. M. Ugaz, D. K. Cinader, W. R. Burghardt, J. P. Quintana, B. S. Hsiao, M. D. Dadmun, W. A. Hamilton and P. D. Butler, *Macromolecules*, 1996, **29**, 5346–5355.
12 M. D. Dadmun and C. C. Han, *Macromolecules*, 1994, **27**, 7522–7532.
13 G. Schmidt, S. Muller, C. Schmidt and W. Richtering, *Rheol. Acta*, 1999, **38**, 486–494.
14 L. M. Walker and N. J. Wagner, *Macromolecules*, 1996, **29**, 2298–2301.
15 P. Butler, *Curr. Opin. Colloid Interface Sci*., 1999, **4**, 214–221.
16 F. S. Bates, K. A. Koppi, M. Tirrell, K. Almdal and K. Mortensen, *Macromolecules*, 1994, **27**, 5934–5936.
17 G. Schmidt, W. Richtering, P. Lindner and P. Alexandridis, *Macromolecules*, 1998, **31**, 2293–2298.
18 N. Ogata, G. Jimenez, H. Kawai and T. Ogihara, *J. Polym. Sci., Part B: Polym. Phys*., 1997, **35**, 389–396.
19 H. Fong, W. D. Liu, C. S. Wang and R. A. Vaia, *Polymer*, 2002, **43**, 775–780.
20 Y. H. Hyun, S. T. Lim, H. J. Choi and M. S. Jhon, *Macromolecules*, 2001, **34**, 8084–8093.
21 S. Pavlikova, R. Thomann, P. Reichert, R. Mulhaupt, A. Marcincin and E. Borsig, *J. Appl. Polym. Sci*., 2003, **89**, 604–611.
22 S. K. Young and K. A. Mauritz, *J. Polym. Sci., Part B: Polym. Phys*., 2002, **40**, 2237–2247.
23 A. Bafna, G. Beaucage, F. Mirabella and S. Mehta, *Polymer*, 2003, **44**, 1103–1115.
24 N. Ogata, S. Kawakage and T. Ogihara, *Polymer*, 1997, **38** 5115–5118.
25 D. J. Chaiko, *Chem. Mater*., 2003, **15**, 1105–1110.
26 R. A. Vaia, S. Vasudevan, W. Krawiec, L. G. Scanlon and E. P. Giannelis, *Adv. Mater*., 1995, **7**, 154–156.
27 J. H. Wu and M. M. Lerner, *Chem. Mater*., 1993, **5**, 835–838.
28 M. Okamoto, P. H. Nam, P. Maiti, T. Kotaka, N. Hasegawa and A. Usuki, *Nano Letters*, 2001, **1**, 295–298.
29 Z. Q. Shen, G. P. Simon and Y. B. Cheng, *Polymer*, 2002, **43** 4251–4260.
30 N. Ogata, S. Kawakage and T. Ogihara, *J. Appl. Polym. Sci*., 1997, **66**, 573–581.
31 D. J. Chaiko, A. Leyva and S. Niyogi, *Adv. Mater. Processes*, 2003, **161**, 44–46.
32 R. A. Vaia, B. B. Sauer, O. K. Tse and E. P. Giannelis, *J. Polym. Sci., Part B: Polym. Phys*., 1997, **35**, 59–67.
33 R. A. Vaia, H. Ishii and E. P. Giannelis, *Chem. Mater*., 1993, **5**, 1694–1696.
34 B. van Duffel, R. A. Schoonheydt, C. P. M. Grim and F. C. De Schryver, *Langmuir*, 1999, **15**, 7520–7529.
35 G. Decher, *Science (Washington, D. C.)*, 1997, **277**, 1232–1237.
36 G. Decher and J. Schlendorff, *Multilayer Thin Films: Sequential Assembly of Nanocomposite Materials*, VCH, Verlagsgesellschaft, 2003.
37 E. R. Kleinfeld and G. S. Ferguson, *Science (Washington, D. C.)*, 1994, **265**, 370–373.
38 E. Loizou, M. M. Malwitz, P. D. Butler, L. Porcar and G. Schmidt, 2004, submitted.
39 G. Schmidt, A. I. Nakatani, P. D. Butler and C. C. Han, *Macromolecules*, 2002, **35**, 4725–4732.
40 G. Schmidt, A. I. Nakatani, P. D. Butler, A. Karim and C. C. Han, *Macromolecules*, 2000, **33**, 7219–7222.
41 G. Schmidt, A. I. Nakatani and C. C. Han, *Rheol. Acta*, 2002, **41**, 45–54.
42 M. M. Malwitz, S. Lin-Gibson, E. K. Hobbie, P. D. Butler and G. Schmidt, *J. Polym. Sci., Part B: Polym. Phys*., 2003, **41**, 3237–3248.
43 Single films with an average layer thickness of a few microns were obtained by manually spreading the filled polymer gel on a glass substrate with a blade. Every few hours one film was spread and dried, which gives *ca*. 7 to 10 layers a day. During the drying process the films were manually oriented by re-spreading the already half-dried films. Samples were dried in desiccators overnight. Films with the same spread direction were dried layer by layer onto each other until a total multilayer film of *ca*. 1 mm was obtained. Then the total thickness was measured with a caliper and divided by the number of layers. This procedure was done for several samples giving thicknesses of 5–7 microns for each single film. The film uncertainty is *ca*. 20% and was calculated as an average from several samples. A mechanical spreader could not be used due to high viscosity and chewing gum like sample behavior.
44 C. J. Glinka, C. J. Barker, B. Hammouda, S. Krueger, J. J. Moyer and W. J. Orts, *J. Appl. Crystallogr*., 1998, **31**, 430–445.
45 G. Bar, Y. Thomann, R. Brandsch, H. J. Cantow and M. H. Whangbo, *Langmuir*, 1997, **13**, 3807–3812.
46 M. H. Whangbo, J. Ren, S. N. Magonov, H. Bengel, B. A. Parkinson and A. Suna, *Surf. Sci*., 1995, **326**, 311–326.
47 V. Ferreiro and G. Coulon, *J. Polym. Sci., Part. B: Polym. Phys*., 2004, **42**, 687–701.
48 M. M. Malwitz, P. D. Butler, L. Porcar, D. P. Angelette and G. Schmidt, *J. Polym. Sci., Part B: Polym. Phys*., 2004, in press.
49 E. R. Kleinfeld and G. S. Ferguson, *Chem. Mater*., 1995, **7**, 2327–2331.
50 P. H. Hermans, J. J. Hermans, D. Vermaas and A. J. Weidinger, *J. Polym. Sci*., 1947, **3**, 393–406.
51 P. H. Hermans, *Kolloid Z*., 1941, **97**, 223–228.
52 J. de Booys and P. H. Hermans, *Kolloid Z*., 1941, **97**, 229–231.
53 J. Bujdak, E. Hackett and E. P. Giannelis, *Chem. Mater*., 2000, **12**, 2168–2174.

